

Final Scientific Report**Project Title:** Hydrogen Storage at Ambient Temperature by the Spillover Mechanism**Project Period:** February 1, 2005 to June 30, 2010**Date of Report:** July 26, 2010**Recipient:** Department of Chemical Engineering, University of Michigan**Award Number:** DE-FC36-05G015078**Working Partners:** Hao Chen, Thomas R. DiRaimondo, Anthony J. Lachawiec, Jr., Yingwei Li, Nick Stuckert, Lifeng Wang, Yuhe Wang, Ralph T. Yang, Jesse Adams, Michael Heben, Anne Dillon, Lin Simpson, Thomas Gennett, Yufeng Zhao, Boris Yakobson, Mike Chung, Hansong Cheng, Alan Cooper, Guido Pez, Yue Wu**Cost-Sharing Partners:** University of Michigan**Contact:** Ralph T. Yang, Phone: 734-936-0771; Email: yang@umich.edu**DOE Managers:** Carole Read, Jesse Adams**1. Executive Summary**

The goal of this project was to develop new nanostructured sorbent materials, using the hydrogen spillover mechanism that could meet the DOE 2010 system targets for on-board vehicle hydrogen storage. Hydrogen spillover may be broadly defined as the transport (i.e., via surface diffusion) of dissociated hydrogen adsorbed or formed on a first surface onto another surface. The first surface is typically a metal (that dissociates H₂) and the second surface is typically the support on which the metal is doped. Hydrogen spillover is a well documented phenomenon in the catalysis literature, and has been known in the catalysis community for over four decades, although it is still not well understood.^{1,2} Much evidence has been shown in the literature on its roles played in catalytic reactions. Very little has been studied on hydrogen storage by spillover at ambient temperature. However, it is also known to occur at such temperature, e.g., direct evidence has been shown for spillover on commercial fuel-cell, highly dispersed Pt/C, Ru/C and PtRu/C catalysts by inelastic neutron scattering.³ To exploit spillover for storage, among the key questions are whether spillover is reversible at ambient temperature and if the adsorption (refill) and desorption rates at ambient temperature are fast enough for automotive applications.

In this project, we explored new sorbents by using a transition metal (e.g., Pt, Ru, Pd and Ni) as the H₂ dissociation source and sorbents as the hydrogen receptor. The receptors included superactivated carbons (AX-21 and Maxsorb), metal organic frameworks (MOFs)

and zeolites. Different metal doping methods have been used successfully to achieve high metal dispersion thereby allowing significant spillover enhancements, as well as a bridging technique used for bridging to MOFs. Among the metals tested, Pt is the hardest to achieve high metal dispersion (and consequently spillover) while Ru is the easiest to disperse. By properly dispersing Pt on superactivated carbons (by following detailed doping and activation conditions given in our publications, e.g., Ref. 12), the storage capacities are increased two-fold (doubled) while slightly more than doubled by Ru doping. The bridging technique remains highly empirical and sample-to-sample consistency is difficult to achieve; however, significant enhancements by spillover can be achieved if the synthesis and pretreatment are done properly. Pitfalls in sample syntheses for both metal doped and bridged sorbents are pointed out in the report; deviations from the synthesis and pretreatment conditions will lead to diminished or no spillover effects.

Due to the high bulk densities of zeolites, metal doped zeolites are shown to be most promising for achieving high volumetric storage capacities by spillover. Kinetics of both spillover and reverse spillover (i.e., desorption) at ambient temperature are also studied. This report summarizes the progress made in the project.

2. Spillover Storage on Metal-doped Superactivated Carbon (AX-21)

The most effective way for achieving spillover on carbon is by direct doping of metal. The crucial factor for spillover on a metal-doped carbon is metal dispersion; a high metal dispersion is necessary for effective spillover.⁴⁻⁶ There are a number of techniques for direct doping; the incipient wetness impregnation technique was used in this project. Since missteps can be made easily, and each misstep will lead to reduced or no spillover, the key steps are summarized below and common missteps are noted. Doping of Pt on AX-21 is used for example. By following this procedure, Pt metal particles in the 1-3 nm sizes are obtained.

- Measure 200mg dry AX-21 or Maxsorb (dried at 393K). Add acetone until all particles are completely dissolved in a very dilute slurry (~20-100mL) (*a more dilute solution increases metal dispersion and hence the spillover enhancement*).
- Dissolve 26 mg H₂PtCl₆ (Aldrich, 99.9%) in at least 20mg acetone and add at a consistent drop wise rate over at least 10 min while stirring vigorously (*using overly concentrated Pt precursor solution and/or faster mixing will lead to poor and UNEVEN metal dispersion and substantially less spillover*). Stir vigorously for at least 10 min after the last drop is added.
- Sonicate (100 W, 42 kHz) the solution for 1 hour and then evaporate the excess liquid in an oven at 333K (allowing the solution to fully dry, e.g. by drying at temperatures higher than 333K, will lead to lowered enhancement).
- Dry the sample further in a quartz tube under He flow at 393K for 2 h. Change the flow to H₂ and raise the temperature to 573K at 1K/min and hold for at least 2 h (*holding for long times ensures complete reduction of Pt*). Switch the flow to He to purge (*purge for at least 4 h and cool at a rate no larger than 1K/min, otherwise Pt will react with air vigorous during sample transfer leading to poor metal dispersion*). The flowrates of H₂/He are not important.
- Sample is transferred to measurement system, using a degas procedure of 623K and a heating rate of no more than 5K/min under vacuum for 8 hours. (Degas at only 573K is not adequate since spiltover hydrogen during H₂ reduction will remain on the carbon surface.)
- In H₂ measurement, the leak rate that is acceptable for physisorption measurement is not acceptable for spillover measurement, and allowing large dead spaces (in sample or reservoir cells) will lead to large errors.

The detailed design and construction of a volumetric system for high pressure measurements have been described elsewhere.⁷ Correction for He adsorption was also described in detail.⁷

Typical and consistent results on hydrogen isotherms at 298K on 6wt% Pt/AX-21 are shown in Figure 1. From the small standard deviation, consistency of the sample preparation is seen.

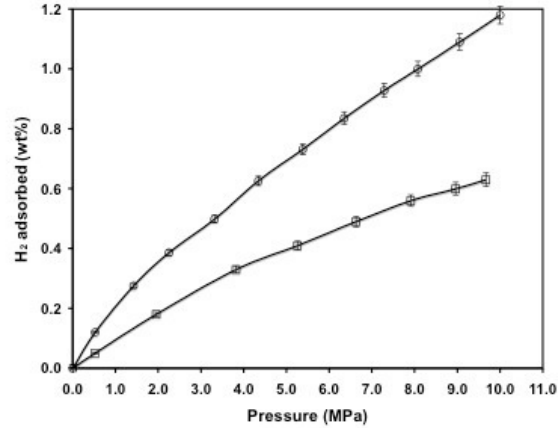


Figure 1. High-pressure Hydrogen Isotherms at 298K on 6 wt%Pt/AX-21 (O, upper curve) by direct doping technique (error bars are based on 1σ of 4 separately prepared samples). Undoped AX-21 (□, lower curve).

The kinetics and mechanism of hydrogen spillover have also been investigated.^{4, 8} It was found that hydrogen molecules were dissociated rapidly on metal sites and then diffused slowly away from them to the receptor. Surface diffusion of hydrogen atoms has been proposed to be the rate-determining step in hydrogen spillover. Thus, by assuming that the surface diffusivity was not dependent on surface concentration, a phenomenological equilibrium isotherm equation was derived for spillover systems:^{4, 9}

$$q = \frac{k_1 \sqrt{P_{H_2}}}{1 + k_2 \sqrt{P_{H_2}} - k_3 \sqrt{P_{H_2}}} \quad (1)$$

All of the constants involved could, in principle, be measured independently. The shape of the isotherm is determined by the relative magnitudes of the two terms in the denominator. At very high pressures, the adsorption amount q will approach a constant (corresponding to saturation adsorption capacity):

$$q \cong \frac{k_1}{k_2 - k_3} \quad (2)$$

The apparent heats of adsorption (ΔH_{ads}) were calculated from the temperature dependence of the isotherms via the Clausius–Clayperon equation, and were -23.3 KJ/mol (at 0.020 wt%), -16.6 KJ/mol (at 0.025 wt%) and -15.1 KJ/mol (at 0.031 wt%).

2.1. Kinetics of Spillover on Pt/AX-21 or Pt/Carbon

The kinetics of adsorption and desorption was measured as percent completion (or fractional completion) during each pressure changing step. Figure 2 shows the adsorption and desorption kinetics on Pt/AX-21 at various end pressures (5-100 atm) and 298K.

As can be seen, the desorption rates are always higher than that of adsorption, and that the rates decreased with hydrogen loading. Although the adsorption or 'charge' rates are low, a large fraction of adsorbed amount was adsorbed in the initial stage, within a few minutes, while the completion of spillover was slow.

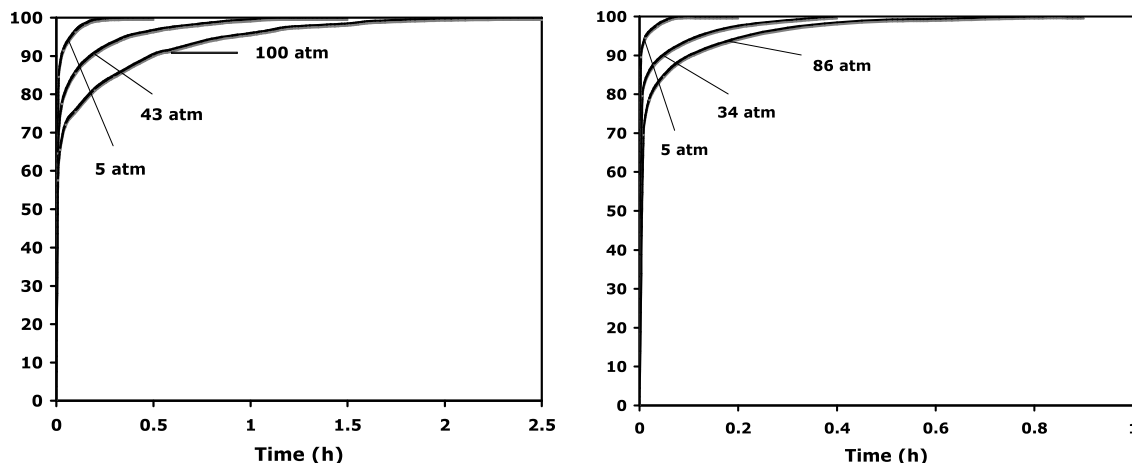


Figure 2. Rates of adsorption (a), and desorption (b) at different pressures on the Pt/AX-21 sample ($T = 298\text{K}$).⁴

In order to understand the kinetics, D_2 isotope tracer was also studied.⁸ A templated carbon (TC) with a BET surface area of $3400\text{ m}^2/\text{g}$ was used. Desorption kinetics were faster relative to adsorption for hydrogen and deuterium on all carbon-based adsorbents in the study. The reason was that the experimentally measured adsorption rates (using either volumetric or gravimetric techniques) do not account for recombination, while desorption rates include both reverse spillover and recombination. Here, recombination refers to the recombination of H atoms on the carbons surface and the subsequent desorption to the gas phase as H_2 . Thus, subtraction of the two rates yields the rate of recombination for hydrogen or deuterium atoms on the carbon surface.

The rates could also be expressed in terms of the surface diffusion time constants, D/R^2 , here D is the diffusivity and R is the reachable distance for the spillover hydrogen from each Pt dissociation center. The diffusion time constants for adsorption and desorption for Pt/TC are shown in Figure 3. The recombination rates, which were the difference between the adsorption and desorption rates, are shown in Figure 4. The results have been explained elsewhere.¹⁰

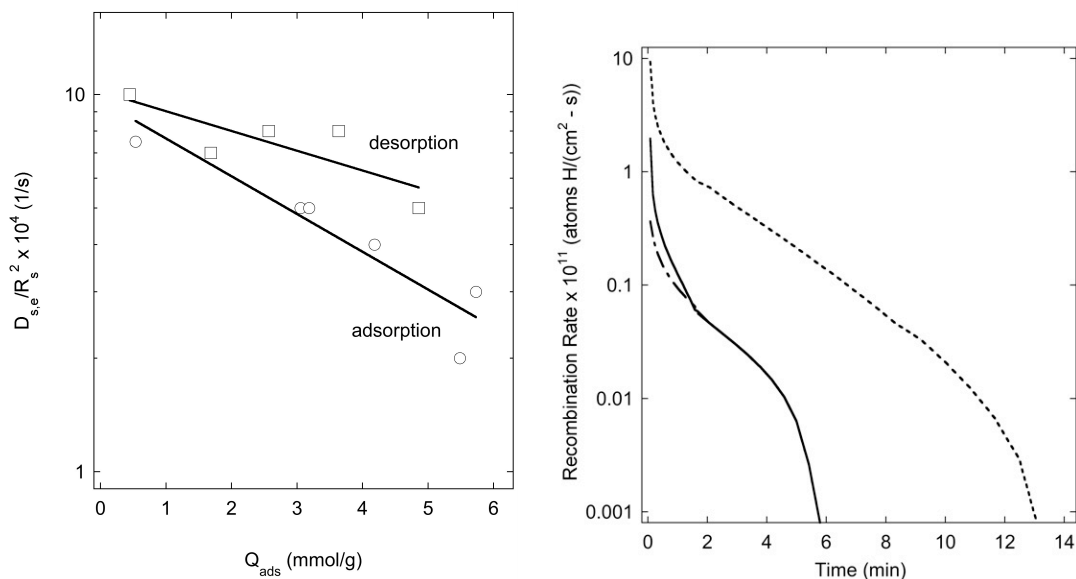


Figure 3 (Left). Diffusion time constants for primary spillover of H on 6 wt% Pt/TC at 298K.⁹

Figure 4 (Right). Rates of hydrogen recombination for primary spillover during equilibration time for final adsorbed amount: 4.5 mmol/g (solid-dashes), 3.5 mmol/g (solid), 0.5 mmol/g (dashes).¹⁰

2.2. Mechanism of Spillover (Adsorption) and Reverse Spillover (Desorption)

In order to obtain a better understanding for the spillover storage mechanism, deuterium isotope tracer and TPD studies were performed on a Pt/TC sample. The Pt/TC sample was subjected to sequential dosing of H₂ and D₂ at 298K, followed by quenching in liquid N₂, shallow evacuation and TPD. Typical results are shown in Figure 5. In this run, 0.4 atm H₂ was dosed first for 5 min. at 298K, followed by dosing with 0.4 atm D₂ for 5 min. The TPD result is shown in Figure 5. The TPD result showed clear desorption peaks of D₂, HD and H₂, in the reversed sequence of dosing. Importantly, a large desorption peak of HD occurred. Detailed results on calibration experiments, other dosing sequences, etc. are shown elsewhere.¹¹ The results are direct evidence to show that (1) atomic species are formed during spillover storage, and (2) the desorption step follows a reverse spillover process, i.e., atoms migrate back to the metal particle, on which to recombine and desorb as molecules.

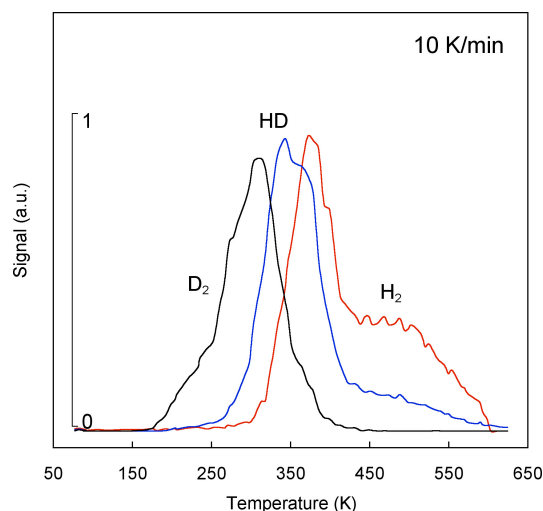


Figure 5. TPD Result for 6 wt% Pt on Templated Carbon (3400 m²/g) after dosing with 0.4 atm H₂ followed by D₂ at 298K for 5 min (followed by quench, gas phase removal and TPD).¹¹

2.3. Comparison of Different Metals

Using the templating approach, and using EMC-2 zeolite as the template (developed at Mulhouse University, France), a nanostructured carbon with a BET surface area of 3839 m²/g was synthesized. The carbon was doped with nanoparticles of different metals (Ru, Pt and Ni). The spillover storage isotherms at 298K are shown in Figure 6.¹² The storage capacities for the doped carbons followed the order of the hydrogen isotherms on pure metal powders: Ru > Pt > Ni. The doped samples were subjected to the standard H₂ reduction post-treatment: 300°C (597K) in H₂. We then used a high temperature thermal reduction technique for the post-treatment: 900°C (1197K) in N₂ (1 hr), marked by Ru/TC-T in Figure 6. Although the BET surface area of this sample was reduced by nearly 50% because of the high temperature treatment, the spillover storage capacity was significantly increased. Further examination of the samples showed that the metal nanoparticles were anchored deeper into the carbon surface by the thermal reduction step (shown clearly by TEM images), hence more spillover.¹²

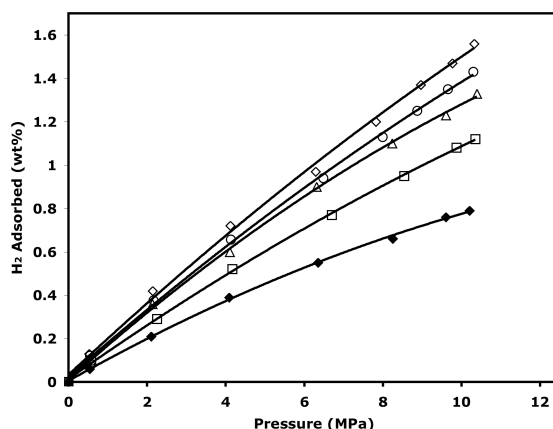


Figure 6. H₂ isotherms at 298K on TC (templated carbon) & 6wt% metal-doped (ultrasound assisted) M/TC. All M/TC were H₂-reduced at 300°C except Ru/TC-T was thermally reduced (in N₂) at 900°C (1 hr) (◇). BET S. A. (m²/g): Ru/TC-T = 2090 (◇); Ru/TC = 3004 (○); Pt/TC = 3120 (△); Ni/TC = 3091 (□); TC = 3839 (◆).¹²

2.4. Effects of Gaseous Impurities in H₂ and Carbon Surface Oxygen Groups on Spillover Storage

In this section, we show the significant increase in spillover by adsorbing an impurity that is commonly found in H₂ such as CH₄. Clearly, the adsorbed CH₄ molecules serve as bridges for hydrogen spillover. The results also illustrate the significant errors in using the Berson-Boudart method (for estimating the metal dispersion of supported metals) when spillover occurs, particularly that enhanced by gas impurities. All of the adsorbents used in this work were prepared by impregnating a support with chloroplatinic acid (H₂PtCl₆) (Aldrich, 99.9%).

In order to investigate the effect of methane molecules on the spillover of hydrogen from the Pt surface to the AX-21 carbon surface, CH₄ was presorbed at predetermined pressures before H₂ isotherms were measured, as described in the foregoing. The results are shown in Figure 7 and Table 1. Figure 7 shows the effect of methane on hydrogen adsorption. The adsorption capacity of H₂ on Pt/AX-21 varied with the initial pressure of methane. Presorbing with methane in the range of 5.0×10⁻⁴ to 3.4×10⁻³ atm resulted in significantly increased adsorption of H₂. From Figure 7 and Table 1, it is seen that the spillover-adsorption amount of H₂ reached the highest value when the initial pressure of methane was at 1.2×10⁻³ atm. At 1.2×10⁻³ atm of methane, the equilibrium adsorption amount of H₂ at 1 atm increased to 8.81 cm³/g STP from 4.78 cm³/g STP without methane, i.e., nearly doubled.

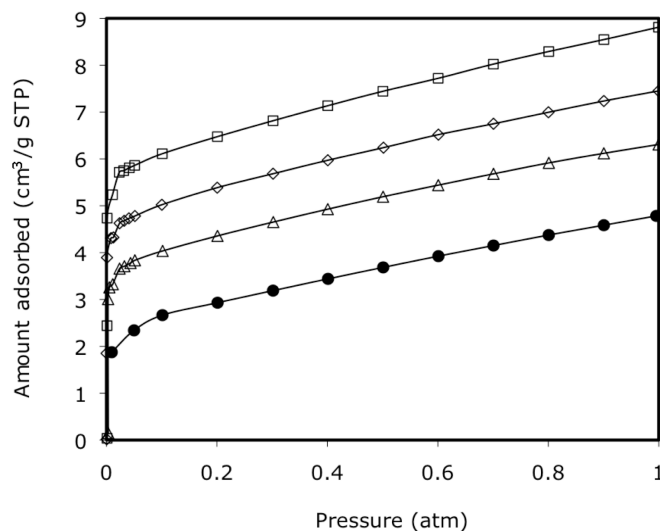


Figure 7. Adsorption isotherm of H₂ on Pt/AX-21 at 298K with presorbed CH₄ at P(CH₄) = 0 (●), 5.0×10⁻⁴ (◇), 1.2×10⁻³ (□) and 3.4×10⁻³ atm (△). The 3 presorbed CH₄ points fall essentially on the origin due to the large Y-axis scale.¹³

Table 1 Results of CH₄ and H₂ adsorption on Pt/AX-21

initial pressure of CH ₄ (atm)	saturation amount of CH ₄ (cm ³ /g, STP) ^a	saturation amount of H ₂ (cm ³ /g, STP) ^b	chemisorption amount of H ₂ (cm ³ /g, STP) ^c	platinum dispersion (%)
0	-	4.78	2.52	73
5.0×10 ⁻⁴	1.5×10 ⁻²	7.45	4.92	143
1.2×10 ⁻³	3.7×10 ⁻²	8.81	5.93	173
3.4×10 ⁻³	15×10 ⁻²	6.03	3.92	114

^a the saturation amount of CH₄ was obtained at the corresponding initial pressure of CH₄.

^b the saturation amount of H₂ was obtained at 1.0 atm of H₂.

^c the chemisorption amounts of H₂ adsorption was obtained at the equilibrium pressure of H₂ extrapolated to zero.

From the adsorbed amount of hydrogen extrapolated to zero pressure, the dispersion of Pt metal on AX-21 can be calculated according to the method of Benson-Boudart. The adsorption of pure hydrogen on AX-21 was by physical adsorption because the adsorption capacity at zero pressure by extrapolating the isotherm was ~0 cm³/g STP (see Figure 8). The chemisorption amount at zero pressure on Pt/AX-21 was 2.52 cm³ STP/g (see Figure 1

and Table 2). Using the assumption of one H per surface Pt atom, the dispersion using pure H₂ was 73%. However, the dispersion exceeded 100% when H₂ contained a small amount of CH₄ (see Table 1). At 1.2×10^{-3} atm of CH₄, the dispersion reached 173% because of the enhanced spillover over CH₄ bridges. Likewise, the dispersion reached 143 and 114% when the initial pressures of methane were at 5.0×10^{-4} and 3.4×10^{-3} atm, respectively. At still higher pressures of CH₄, competitive adsorption between H and CH₄ occurs, i.e., competition for the most energetic sites, as is the case in all binary mixture adsorption. Such was the case for CH₄ at 3.4×10^{-3} atm. For the pure AX-21, no hydrogen spillover or the promotion effect of CH₄ on hydrogen adsorption was found (see Figure 7).

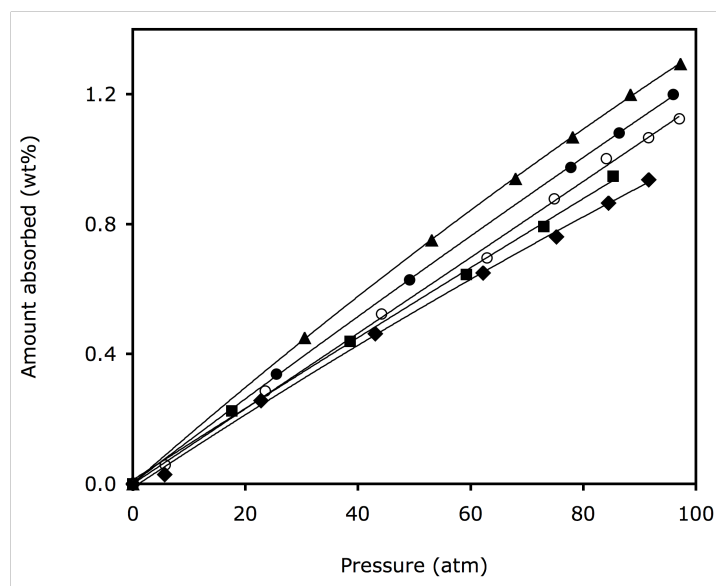


Figure 8. Adsorption isotherm of H₂ on Pt/AX-21 at 298K with presorbed CH₄ at P(CH₄) = 0 (○), 1.0×10^{-3} (●), 5.0×10^{-3} (▲), 1.0×10^{-2} (■), and 0.1 atm (◆).¹³

For H₂ storage, high-pressure isotherms were also measured, and the results are shown in Figure 8. Figure 8 shows that the capacity of pure hydrogen on Pt/AX-21 was 1.20 wt% at 25°C and 100 atm, which was the same with our previous work. The effect of methane on the H₂ storage at high pressures was similar to that at < 1 atm. The greatest H₂ storage on Pt/AX-21 appeared at 5.0×10^{-3} atm of the initial CH₄ pressure. Increasing or decreasing the initial pressure of methane, the adsorption amounts of hydrogen decreased. When the pressure of methane was at 5.0×10^{-3} atm, the H₂ storage reached 1.38 wt%, which was ~15% higher than that of pure H₂ adsorption. Taking the area per surface carbon atom as 8.2 \AA^2 , 0.21 H atom was adsorbed per C atom at 100 atm without CH₄ impurity. By preadsorbing CH₄, the density increased to 0.24 H/C.

One of the factors determining the spillover-storage amounts is the surface chemistry of the receptor. For carbon, doping by heteroatoms including oxygen may have strong effects. Introducing surface oxygen groups may also have effects. The heteroatom in doped carbon increased the interactions between the receptor and hydrogen, and thus led to enhanced

hydrogen adsorption. One may expect therefore, a receptor exhibiting stronger interaction with hydrogen molecules or atoms would be favorable for hydrogen adsorption. In a hydrogen spillover system, the presence of oxygen groups (as will be shown in our molecular orbital calculations) leads to stronger adsorption for the spillover hydrogen, thus an enhanced storage capacity could be expected on an oxygen modified carbon receptor. However, the effect of oxygen in carbons on hydrogen storage via spillover has not been reported. Carbon materials with oxygen groups can be obtained by oxygen doping or direct synthesis. Compared with boron or nitrogen doping, addition of surface oxygen groups to a carbon receptor is an easy process. As for direct synthesis, graphite oxide is a well-known carbon material with abundant oxygen groups. Since the first report in 1855 on the synthesis of graphite oxide by oxidizing graphite with $\text{KClO}_3/\text{HNO}_3$, graphite oxide has been prepared through various routes and studied by many authors. By considering these aspects, we prepared two different carbons of super-activated carbon (AX-21) and graphite oxide doped with Pd metals, and investigated the effects of surface oxygen in these carbons on hydrogen storage via spillover.

The following three doped carbons were first prepared (using NaBH_4 as the reducing agent): 10 wt% Pd doped on AX-21 (Pd/AX-21), 10 wt% Pd doped on Oxygen modified AX-21 (Pd/AX-21-O), and 10 wt% Pd doped on graphite oxide (Pd/graphite oxide). Elemental analysis by XPS (O/(C+O): w/w) indicated oxygen content in Pd/AX-21-O was about 13 wt%, while that in the Graphite Oxide was approximately 40 wt%.¹⁴

High-pressure hydrogen isotherms at 298K for plain AX-21, Pd/AX-21 and Pd/AX-21-O samples are shown in Figure 9. In Figure 9, AX-21 exhibited a hydrogen storage capacity of 0.61 wt% at 298K and 10 MPa, which is in agreement with previous results. By doping 10 wt% Pd on AX-21 sample, the hydrogen uptakes on Pd/AX-21 and Pd/AX-21-O at 10 MPa were enhanced to 0.98 and 1.15 wt %, respectively. It can be seen that both Pd/AX-21 and Pd/AX-21-O samples exhibited much higher hydrogen adsorption capacities than the plain AX-21 sample. The enhanced hydrogen storage capacity cannot be attributed to the differences in surface area because the doped samples have, in fact, lower surface areas than plain AX-21, as is evident from nitrogen adsorption results. The enhancement in hydrogen storage was due to the spillover of atomic hydrogen from metal particles to AX-21. The enhanced hydrogen storage by metal-doped on carbon materials have been observed. It is significant that Pd/AX-21-O had a higher storage capacity than Pd/AX-21. Normalized by the BET surface area, the Pd/AX-21-O adsorbed 22% more hydrogen than Pd/AX-21. The surface oxygen groups on Pd/AX-21-O were responsible for this enhanced capacity. The enhancement is much stronger for graphite oxide. For 1000 m^2/g surface area of Pd/graphite oxide, the amount of spillover storage is 1.4 wt%. The result is significant for meeting the DOE targets.

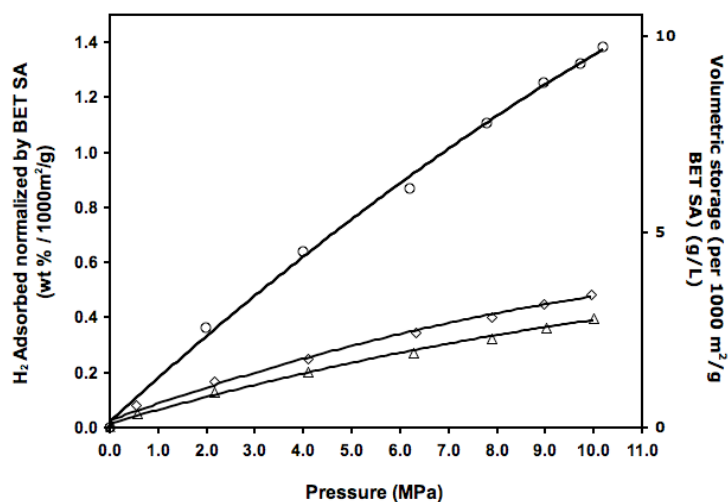


Figure 9. High-pressure hydrogen isotherms at 298K for 10% Pd/graphite oxide (○), 10%Pd/AX-21-O (◇) and 10% Pd/AX-21 (△), normalized by BET surface area. The BET surface areas are: 2466 m²/g for Pd/AX-21 and 2362 m²/g for Pd/AX-21-O, and 687 m²/g for Pd/graphite oxide.¹⁴

An effective way to add oxygen functional groups on carbon surfaces is by O₂ plasma treatment. A templated carbon (TC) was thus treated, designated as TC-Plasma. It was treated with a glow discharge plasma. The pressure in the plasma cell was adjusted to the range 100-200 Pa, and the glow discharge plasma was generated by applying 5000 V to the electrodes using a DC high voltage generator with oxygen as the plasma forming gas. Details are described elsewhere.¹⁵

It is shown that the enhancement is greater by oxygen plasma treatment compared to air oxidation, because different surface groups were formed. The surface groups were determined by XPS. Oxygen plasma treatment generated mainly semiquinone (C=O) groups while air oxidation formed mainly hydroxyl (C-OH) groups. Experimental heats of adsorption, XPS analyses and *ab initio* molecular orbital calculations showed that the binding energies between the spillover hydrogen and different groups followed the order: Lactone > Semiquinone > Carboxyl > Basal Plane. Thus, the H₂ storage capacity at 298K and 10 MPa was increased from 1.17 wt% (without O₂ treatment) to 1.74 wt% on Pt-doped on a templated carbon that was pretreated with O₂ plasma. However, there was a decrease in storage capacity during the first three adsorption-desorption cycles (at 298K and 10 MPa). The results are shown in Figures 10, 11 and Table 2. The capacity decreased from 1.74 wt% to 1.30 wt% and remained unchanged after three cycles. XPS results showed that this decrease was caused by the very strong (and irreversible) binding of the spillover hydrogen with the lactone groups (HO-C=O). Nonetheless, the main groups of semiquinone remain functional as receptor sites upon cycling and the 1.32 wt% storage capacity is among the highest reversible capacities reported in the literature.

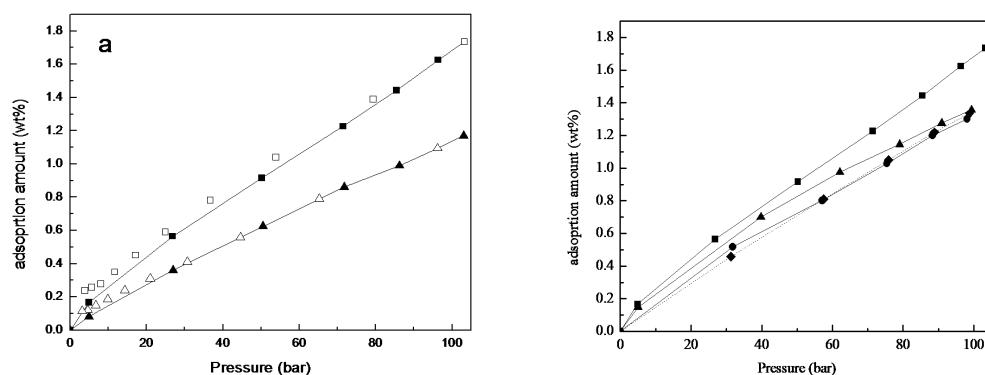


Figure 10 (Left). High-pressure hydrogen isotherms at 298K for 6wt% Pt doped on various carbons. Adsorption (■) and desorption (□) on Pt/TC-O (via O₂ plasma); Adsorption (▲) and desorption (△) on Pt/TC (not oxidized).¹⁵

Figure 11 (Right). Cyclic adsorption/desorption of H₂ on 6wt% Pt/TC-Plasma: First cycle (■, 1.75wt% at 100 atm); 2nd cycle (▲) 1.36wt%; 3rd cycle (●) 1.32wt%; and 4th cycle (◆) 1.32wt%.¹⁵

Table 2. XPS relative subpeak area of C_{1s} of the untreated and oxygen plasma treated carbon¹⁵

S.A. and XPS (C _{1s} Rel. Area)	TC	TC-Plasma	Pt/TCPlasma th 4 cycle
BET S.A., m ² /g	3554	3110	
C-C (284.6eV)	89.43%	65.08%	67.53%
C-OH (286.1eV) Hydroxyl	4.61%	5.72%	6.37%
C=O (287.6eV) Semiquinone	3.77%	25.76%	25.13%
-O-C=O (289.6eV) Lactone	2.19%	3.44%	0.97%

2.5. Catalysts for Increasing the Rates of Spillover⁶

In order to increase the rates of spillover, we explored the doping of metal salts to study possible catalytic effects of, e.g., TiF₃, on hydrogen spillover on Pt-doped carbon.⁶ By doping 2wt% TiF₃, the rates for both adsorption and desorption were significantly increased. The results are summarized in Figure 12. The rates were monitored at different pressure increasing or decreasing steps. Figure 12 shows only one of such steps. The results for other steps were similar. The H₂

isotherms on the Pt/maxsorb and metal salt doped samples were similar, with slight decreases in the amounts adsorbed caused by the slightly lower BET surface areas upon TiF_3 doping. The rates were expressed in terms of fractional completion versus time upon each pressure increase step. Here, Pt/Maxsorb- TiF_3 (473K) denotes that the doped sample was heat treated at 473K, while the other sample was heat treated at 673K. XPS results indicated that C-F bonds were formed in the sample and that the sample heat treated at 673K had more C-F bonds, and consequently stronger catalytic effects.⁶

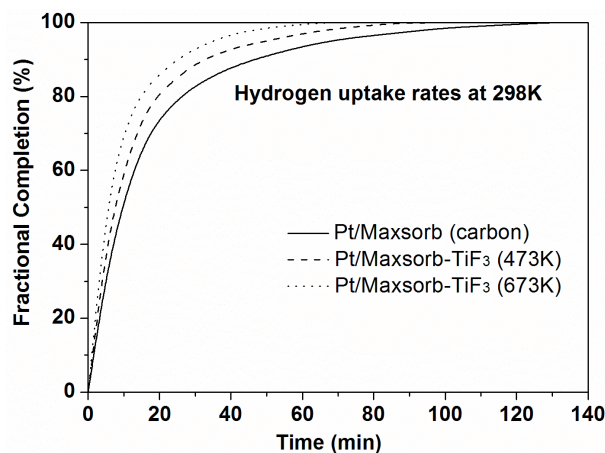


Figure 12. Hydrogen desorption rates on Pt/Maxsorb, Pt/Maxsorb- TiF_3 -A and Pt/Maxsorb- TiF_3 -B at 298K. Pressure step: (a) 77.7-52.8 atm for Pt/Maxsorb; (b): 78.1-53.1 atm for Pt/Maxsorb- TiF_3 -A; (c) 77.9-52.9 atm for Pt/Maxsorb- TiF_3 -B.

3. Spillover to Metal Organic Frameworks (MOFs)

Strong effects of bridging materials on spillover were discovered soon after the discovery of the spillover phenomenon.^{16,17} In this project, we developed a strategy to form carbon bridges between the spillover catalyst source (such as Pt/AC) and MOF particles, using sugar as the precursor for carbon bridges. Details of the approach have been given elsewhere.¹⁸ A summary is given below. Common pitfalls in the synthesis of the bridged material are also discussed.

3.1. Synthesis of IRMOF-8

The method of Huang, et al.¹⁹ was used to synthesize IRMOF-8 and IRMOF-1. Using Yaghi's method²⁰ would yield large crystals and will not work for bridging due to the large crystal sizes that are incompatible with the small Pt/AC sizes. The sizes of the IRMOF-8 and IRMOF-1 were in the range of 100-200 nm, which were comparable to that of the Pt/AC catalyst, while Yaghi's recipe will yield large crystals of ~100 microns, and no spillover will be seen.

1. $\text{Zn}(\text{NO}_3)_2 \cdot 6\text{H}_2\text{O}$ (1.19 g, 4 mmol, must be freshly opened) and 2,6-naphthalenedicarboxylic acid (0.43 g, 2 mmol) were dissolved in 40 ml of dimethylformamide (DMF) during vigorous stirring at room temperature.
2. Three drops of H_2O_2 aqueous solution (30 wt %) was added to the solution. Triethylamine (2.3 ml) was slowly added dropwise to the above solution under vigorous agitation for 1 h. (one drop/30 seconds, to deprotonate the acid to initiate polymerization)
3. The white product was collected by repeated filtering, thorough washing with DMF for three times. The sample was degassed first at room temperature for 6 h, then heated to 180°C at a heating rate of 1°C/min and held at that temperature for 12 h under degassing in vacuum. (boiling point of DMF is 153°C)

3.2. Preparation of bridged samples and sample pretreatment for isotherm measurement:

1. IRMOF-8 (200 mg), 10 % Pt/AC catalyst (25 mg), and sucrose (33.2 mg) were ground together for 1 h. (very gentle "grinding" with mortar and pestle to achieve uniform mixing; ball-milling may destroy the structure due to high energy), particle size compatibility is important
2. This mixture was transferred to a quartz boat that was placed in a tubular reactor. The mixture was heated in flowing helium (100 mL/min) at a heating rate of 1°C /min to 200°C and held at this temperature for 3 h. (pile sample in the quartz boat – not spreading as a layer. Melting point of sucrose: 186°C)
3. Subsequently the temperature was increased at 1°C /min to 250°C and held for 12 h. The material was cooled to room temperature at 1°C /min in flowing helium. (Higher temperature could destroy the structure of MOFs)

4. The samples were stored in vacuum before being moved into the sample holder for high-pressure measurements. (avoid or minimize any possible decomposition of MOFs by exposing to ambient air)
5. Approximately 200 mg of sample was used for isotherm measurement. Prior to measurements, the samples were degassed in vacuum at 200°C for 24 h. Pretreatment at lower temperatures would not be adequate to activate the catalyst.

However, it is noted that consistency of spillover storage on the bridged MOF samples is difficult to achieve due to the empirical nature of bridge building.^{21, 22} As shown in Figure 13, the storage capacity of the bridged IRMOF-8 varies from sample to sample, which is due to the different particle connectivities among each sample, and how thoroughly the catalyst and MOF particles are mixed. The key factors in sample preparation that affect storage capacity have been discussed elsewhere.^{21, 22} It is also noted that our best data have been reproduced by at least 3 groups (Ref. 21-23). The work of Liu et al. is particularly interesting, as they achieved high enhancements by properly bridging MIL-101 and MIL-53 (enhancement factors of 3 and 13, respectively). In summary, significant enhancements will be obtained if all bridging steps are followed properly.^{21, 22}

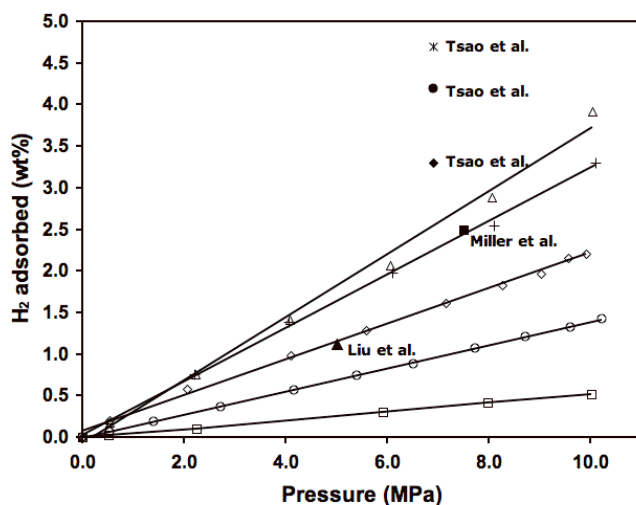


Figure 13. Storage capacities of various bridged IRMOF-8 samples and pure IRMOF-8 (\square).^{21, 22} Data points from the literature are also shown for comparison: Tsao et al. (Ref. 23) and Miller et al. (\blacksquare Ref. 24). The data point from Liu et al. (\blacktriangle Ref. 25) is for bridged MIL-101. See text for successful spillover on bridged MIL-53 and MIL-101.

4. Spillover to Zeolites – Toward DOE Volumetric Targets²⁶

Because of the high bulk densities of zeolites which are substantially higher (2-3 times higher) than that of carbons and metal organic frameworks, plus the high densities of cation sites on a variety of zeolites, zeolites are promising sorbents for achieving high volumetric storage capacities.

Hydrogen adsorption properties of low-silica type-X zeolites (LSX, Si/Al = 1)²³ containing alkali or alkali-earth metal cations (Li^+ , Ca^{2+} , and Mg^{2+}) have been studied in this project. Li-LSX is commercially used for air separation.²⁷ It was found that the hydrogen adsorption capacities of LSX zeolites at 77K were determined mainly by the porosity of the zeolite, while at 298K, the storage capacities depended on both the H_2 -cation interactions and the porosity. Among the three exchanged zeolites, Li-LSX had the highest H_2 capacity of 1.5 wt % at 77K and 1 atm, and Ca-LSX had the highest capacity of 0.50 wt % at 298K and 10 MPa.

Hydrogen storage in LSX zeolites via spillover was also investigated.²⁶ Three methods including bridge building with a catalyst, metal doping via incipient wetness impregnation and metal doping via chemical vapor deposition (CVD) were employed to induce hydrogen spillover and enhance the storage capacities. Thus, the storage capacities were increased to 0.96-1.2 wt % on the Pt-doped zeolites at 298K and 10 MPa. The differences between the three methods were compared and discussed.²⁶ Furthermore, 5 and 10 wt % Ni were doped on Ca-LSX zeolite. The 10 wt % Ni-doped Ca-LSX zeolite showed a storage capacity of 1.15 wt % at 100 atm and 298K. The important volumetric storage capacities of these zeolites were also estimated based on the densities of the densified zeolites. 21 g/L was obtained for Pt-doped Ca-LSX and 20 g/L was obtained for Ni-doped Ca-LSX, both at 298K and 10 MPa. The high volumetric capacities were obtained because of the high densities of zeolites which are substantially higher (2-3 times higher) than that of carbons and metal organic frameworks.

4.1. CVD-Pt/Ca-LSX

In the present study, 5 wt % Pt was doped on Ca-LSX zeolite by chemical vapor deposition of the platinum precursor (Trimethyl) methylcyclopentadienyl platinum (IV) and subsequent reduction in a hydrogen atmosphere. The TEM image of CVD-Pt/Ca-LSX showed nanosized Pt (~1-3 nm) were well dispersed on the particles of LSX. The hydrogen adsorption isotherm at 298K (Figure 14) showed that CVD-Pt/Ca-LSX had a storage capacity of 1.20 wt % at 10 MPa, enhanced by a factor of 2.4 compared with that of plain Ca-LSX (0.5 wt %). Reversibility was evaluated by measuring the desorption branch down to 1 atm. The desorption branch nearly followed the adsorption branch although there appeared to be a slight hysteresis. The second adsorption isotherm was in agreement with the first adsorption isotherm. These results indicated that hydrogen adsorption in the CVD-Pt/Ca-LSX was reversible at 298K.

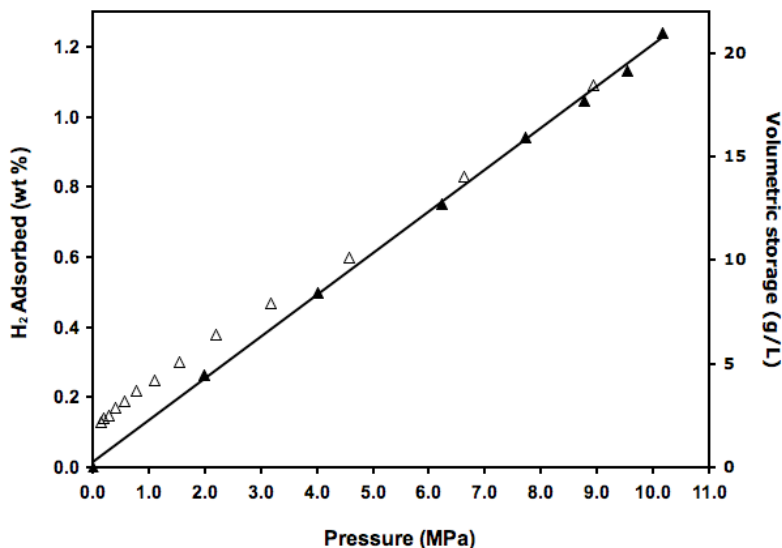


Figure 14. High-pressure hydrogen isotherms on CVD-Pt/Li-LSX (adsorption: ▲; desorption: △) at 298K and 10 MPa.²⁶

4.2 Ni/Ca-LSX

5 wt % Ni was doped on Ca-LSX by incipient wetness impregnation of an aqueous solution of $\text{Ni}(\text{NO}_3)_2 \cdot 6\text{H}_2\text{O}$ and subsequent reduction in a hydrogen atmosphere at 723K. The TEM image showed that black Ni particles were dispersed on the LSX zeolites with sizes around 4-10 nm. The loading amount of Ni on Ca-LSX was further increased from 5 to 10 wt % to increase the dissociation sites. As shown in Figure 15, the 10 wt % Ni/Ca-LSX had a storage capacity of 1.15 wt %. Although the loading amount of Ni was doubled, the storage capacity was not increased much.

The volumetric storage capacity of Ni/Ca-LSX was estimated to be 20 g/L (Figure 15), based on the pellet density of 1.7 g/cm^3 . This indicates Ni/Ca-LSX is a promising sorbent for onboard hydrogen storage.

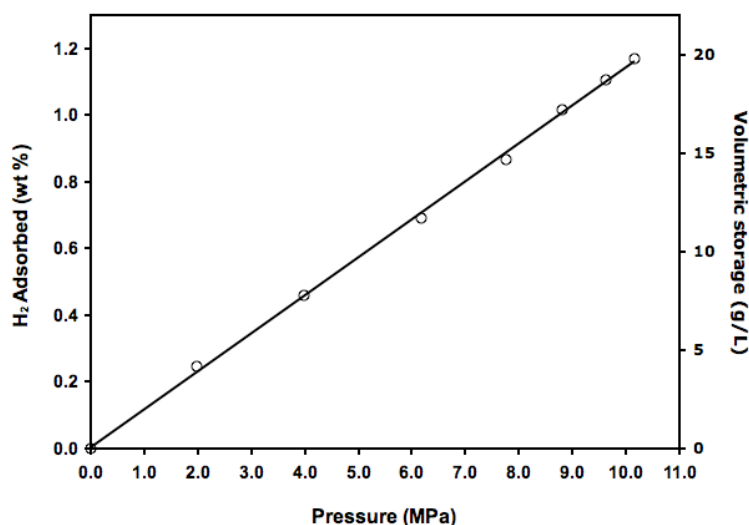


Figure 15. High-pressure hydrogen isotherms on 10 wt % Ni/Ca-LSX (○) at 298K and 10 MPa.²⁶

4.3. Concluding Note

The updated 2010 DOE volumetric system target for onboard storage is 28 g/L at near ambient temperature and 100 atm. The two metal doped zeolites reported here showed 20 and 21 g/L. Unlike MOFs, zeolites are highly stable and low-cost. The Ni-doped zeolites, in particular, are most promising for practical applications after further development.

Up to date, there are approximately 100 published articles reporting significant enhancements by spillover near ambient temperature. These enhancements were achieved by approximately 40 different groups worldwide. Their key results have been reviewed in a forthcoming review.²⁸ Moreover, common pitfalls in sample syntheses and pretreatment for both metal doped and bridged sorbents are pointed out in the report and elsewhere;²¹ deviations from the synthesis and pretreatment conditions will lead to diminished or no spillover effects.²¹

References

- 1 A. J. Robell, E. V. Ballou and M. Boudart, *J. Phys. Chem.* 1964, **68**, 2748.
- 2 W. C. Conner, Jr. and J. L. Falconer, *Chem. Rev.*, 1995, **95**, 759.
- 3 P. C. H. Mitchell, A. J. Ramirez-Cuesta, S. F. Parker, J. Tomkinson, D. Thompsett, *J. Phys. Chem. B.*, 2003, **107**, 6838.
- 4 Y. W. Li and R. T. Yang, *J. Phys. Chem. C.* 2007, **111**, 3405.
- 5 C. S. Tsao, Y. R. Tzeng, M. S. Yu, C. Y. Wang, H. H. Tseng, T. Y. Chung, H. C. Yu, T. Yamamoto, K. Kaneko and S. H. Chen, *J. Phys. Chem. Lett.*, 2010, **1**, 1060.
- 6 H. Chen, R. T. Yang, *Langmuir*, 2010, DOI: 10.1021/la100172b.
- 7 Lachawiec, Jr.; A. J.; DiRaimondo, T. R.; Yang, R. T. *Rev. Sci. Instrum.* 2008, **79**, 063906.
- 8 A. J. Lachawiec, Jr. and R. T. Yang, *Langmuir*, 2008, **24**, 6159.
- 9 Li, Y. W.; Yang, F. H.; Yang, R. T. *J. Phys. Chem. C* **2007**, *111*, 3405.
- 10 A. J. Lachawiec, Jr. and R. T. Yang, *J. Phys. Chem. C.*, 2009, *113*, 13933.
- 11 A. J. Lachawiec, Jr. and R. T. Yang, *Langmuir*, *24*, 6159 (2008).
- 12 L. F. Wang and R. T. Yang, *J. Phys. Chem. C.*, 2008, *112*, 12486.
- 13 Y. H. Wang and R. T. Yang, *J. Catalysis*, *260*, 198 (2008).
- 14 L. F. Wang, F. H. Yang, R. T. Yang and M. A. Miller, *Ind. Eng. Chem. Res.*, **48**, 2920 (2009).
- 15 Z. Wang, F. H. Yang and R. T. Yang, *J. Phys. Chem. C.*, *114*, 1601 (2010).
- 16 W. C. Neikam, M. A. Vannice, *Proc. 5th Intern. Congress on Catalysis*, Vol. 1, pp. 40-609 to 40-619 (1973), North Holland, Amsterdam.
- 17 G. C. Bond, in *Spillover of Adsorbed Species*, (G. M. Pajonk, S. J. Teichner, and J. E. Germain, Ed.) Elsevier, Amsterdam, 1983, pp. 1-16.
- 18 Li, Y.W.; Yang, R. T., *J. Am. Chem. Soc.*, *128*, 8136 (2006).
- 19 L. M. Huang, H. T. Wang, J. X. Chen, Z. B. Wang, J. Y. Sun, D. Y. Zhao, Y. S. Yang, *Microporous Mesoporous Mater.*, 2003, *58*, 105.
- 20 N. L. Rosi, J. Eckert, M. Eddaoudi, D. T. Vodak, J. Kim, W. O'Keefe, O. M. Yaghi, *Science*, 2003, *300*, 1127.
- 21 N. R. Stuckert, L. F. Wang, R. T. Yang, *Langmuir*, *26*, 11963 (2010).
- 22 R. T. Yang, Y. W. Li, A. J. Lachawiec. Hydrogen storage by spillover. FY 2007 Annual Progress Report, DOE Hydrogen Program, US Department of Energy, Washington, D.C., IV.C.1b, 2007, pp. 539-541.
- 23 Tsao, C.S.; Yu, M. S; Wang, C.Y.; Liao, P.Y.; Chen, H.L.; Jeng, U.S.; Tzeng, Y.R.; Chung, T.Y.; Wu, H.C. *J. Am. Chem. Soc.* *131*, 1404 (2009).
- 24 Miller, M.A.; Wang, C.Y.; Merrill, G. N. *J. Phys. Chem. C.*, *113*, 3222 (2009).

- 25 Liu, Y.Y.; Zheng, J-L.; Zhang, J.; Xu, F.; Sun, L-X. *Intern. J. Hydrogen Energy*, 32, 4005(2007).
- 26 L. F. Wang and R. T. Yang, *Ind. Eng. Chem. Res.*, 49, 3634 (2010).
- 27 R. T. Yang, *Adsorbents: Fundamentals and Applications*, Wiley, Hoboken, NJ. 2003, Ch. 7.
- 28 L. F. Wang and R. T. Yang, *Catalysis Reviews*, 54(4), 411-461 (2010).

Appendix (Publications from this project):

- L. F. Wang and R. T. Yang, "Hydrogen Storage on Carbon-based Adsorbents and Storage at Ambient Temperature by Hydrogen Spillover," *Catalysis Reviews – Sci. & Eng.*, 54(4), 411-461 (2010).
- N. R. Stuckert, L. F. Wang and R. T. Yang, "Characteristics of Hydrogen Storage by Spillover on Pt-doped Carbon and Catalyst-Bridged Metal Organic Framework," *Langmuir*, 26, 11963 (2010).
- L. F. Wang and R. T. Yang, "Hydrogen Storage Properties of Low-Silica Type X Zeolites" *Ind. Eng. Chem. Res.*, 49, 3634 (2010).
- H. Chen and R. T. Yang, "Catalytic Effects of TiF_3 on Hydrogen Spillover on Pt/Carbon for Hydrogen Storage," *Langmuir*, DOI: 10.1021/la100172b
- Z. Wang and R. T. Yang, "Enhanced Hydrogen Storage on Pt-Doped Carbon by Plasma Reduction," *J. Phys. Chem. C.*, 114, 5956 (2010).
- Z. Wang, F. H. Yang and R. T. Yang, "Enhanced Hydrogen Spillover on Carbon Surfaces Modified by Oxygen Plasma," *J. Phys. Chem. C.* 114, 1601 (2010).
- L. F. Wang and R. T. Yang, "Hydrogen Storage Properties of N-doped Microporous Carbon" *J. Phys. Chem. C.*, 113, 21883 (2009).
- A. J. Lachawiec, Jr. and R. T. Yang, "Reverse Spillover of Hydrogen on Carbon-Based Nanomaterials: Evidence of Recombination Using Isotopic Exchange," *J. Phys. Chem. C.*, 113, 13933 (2009).
- R. T. Yang and Y. H. Wang, "Catalyzed Hydrogen Spillover for Hydrogen Storage," *J. Am. Chem. Soc.*, 131, 4224 (2009).
- L. F. Wang, F. H. Yang, R. T. Yang and M. A. Miller, "Effect of Surface Oxygen Groups in Carbons on Hydrogen Storage by Spillover," *Ind. Eng. Chem. Res.*, 48, 2920 (2009).
- L. F. Wang, F. H. Yang and R. T. Yang, "Hydrogen Storage Properties of B- and N-Doped Microporous Carbon," *AIChE J.*, 55, 1823 (2009).
- Y. H. Wang and R. T. Yang, "Increased Hydrogen Spillover by Gaseous Impurity - Benson-Boudart Method for Dispersion Revisited," *J. Catalysis*, 260, 198 (2008).
- L. F. Wang and R. T. Yang, "Hydrogen Storage Properties of Carbons Doped with Ruthenium, Platinum and Nickel Nanoparticles," *J. Phys. Chem. C.*, 112, 12486 (2008).

- A.J. Lachawiec, Jr., T. R. DiRaimondo, and R. T. Yang, "A Robust Volumetric Apparatus and Method for Measuring High-Pressure Hydrogen Storage Properties of Nanostructured Materials," *Rev. Sci. Instr.*, **79**, 063906 (2008).
- A. J. Lachawiec, Jr. and R. T. Yang, "Isotope Tracer Study of Hydrogen Spillover on Carbon-Based Adsorbents for Hydrogen Storage," *Langmuir*, **24**, 6159 (2008).
- L. F. Wang and R. T. Yang, "New Sorbents for Hydrogen Storage by Hydrogen Spillover – A Review," *Energy & Environmental Science* (Roy. Soc. Chem. Cambridge), *Invited Featured Review*, **1**, 268 (2008).
- Y. W. Li and R. T. Yang, "Hydrogen Storage in Metal-Organic Frameworks and a Covalent-Organic Framework," *AIChE Journal*, **54**, 269 (2008).
- Y. Li and R. T. Yang, "Gas Adsorption and Storage in Metal-Organic Framework MOF-177," *Langmuir*, **23**, 12937 (2007).
- Y. Li, R. T. Yang, C. J. Liu and Z. Wang, "Hydrogen Storage on Carbon Doped with Platinum Nanoparticles Using Plasma Reduction," *Ind. Eng. Chem. Res.*, **46**, 8277 (2007).
- Y. W. Li and R. T. Yang, "Hydrogen Storage on Platinum Nanoparticles Doped on Super-Activated Carbon," *J. Phys. Chem. C*, **111**, 11086 (2007).
- Y. W. Li, F. H. Yang and R. T. Yang, "Kinetics and Mechanistic Model for Hydrogen Spillover on Bridged Metal-Organic Frameworks," *J. Phys. Chem. C*, **111**, 3405 (2007).
- Y. W. Li and R. T. Yang, "Hydrogen Storage in Low Silica Type X Zeolites," *J. Phys. Chem. B*, **110**, 17175 (2006).
- Y. W. Li and R. T. Yang, "Hydrogen Storage in Metal-Organic Frameworks by Bridged Hydrogen Spillover," *J. Am. Chem. Soc.*, **128**, 8136 (2006).
- F. H. Yang, A. J. Lachawiec, Jr. and R. T. Yang, "Adsorption of Spillover Hydrogen Atoms on Single-Wall Carbon nanotubes," *J. Phys. Chem. B.*, **110**, 6236 (2006).
- Y. W. Li and R. T. Yang, "Significant Enhancement of Hydrogen Storage Capacity in Metal-Organic Frameworks via Spillover," *J. Am. Chem. Soc.*, **128**, 726 (2006).
- A. J. Lachawiec, Jr., G. S. Qi and R. T. Yang, "Hydrogen Storage in Nanostructured Carbons by Spillover: Bridge Building Enhancement," *Langmuir*, **21**, 11418 (2005).